Ordering of amorphous germanium prior to crystallization

M. A. Paesler and Dale E. Sayers
North Carolina State University, Raleigh, North Carolina 27650

Raphael Tsu and Jesus Gonzalez-Hernandez
Energy Conversion Devices, Inc., 1675 West Maple Road, Troy, Michigan 48084
(Received 24 November 1982)

We present the results of Raman and extended x-ray-absorption fine-structure (EXAFS) experiments performed on sputtered amorphous germanium for both as-deposited and postdeposition annealed samples. From the Raman results, shifts in TO-phonon frequency and linewidth associated with relatively low-temperature annealing are interpreted as indications of ordering prior to crystallization. For annealing at 400 °C, we determine from the Raman results that the volume fraction of crystallinity is $\leq 10^{-3}$. From EXAFS results performed on the same samples, indications of ordering prior to crystallization are manifest in the appearance of a second-nearest-neighbor peak. A bond-angle variation of $\Delta\theta = 7° \pm 1°$ was found for the 400 °C-annealed sample. This value of $\Delta\theta$ was determined by comparing the EXAFS data for this sample with models of the amorphous material generated by adding bond-angle distortion to the crystalline data.

I. INTRODUCTION

The disorder-to-order transition in elemental group-IV semiconductors has been studied for many years. Properties as diverse as porosity,[1] electron-spin resonance,[2] magnetic susceptibility,[3] and internal stress[4] have been monitored in attempts to understand the ordering process. Techniques ranging from simple thermal annealing,[1-4] to laser annealing,[5] and to pricking with a sharp point,[6] have been used to induce the transition. Recently, rekindled interest in this amorphous to crystalline transformation has led to new studies[7] and even symposia[8] dedicated to "fundamentals of crystallization of amorphous silicon."

With regards to the pretransition amorphous material it has long been established that the basic tetrahedral bonding unit of the crystal is preserved—a certain density of dangling bonds notwithstanding. As more is learned about the amorphous state more subtle studies of medium-range order[9] and specific kinds of disorder[10,11] (bond-angle changes, dihedral-angle variations, and bond-length distortions) have gained new prominence. While some studies have involved extant crystalline regions as they grow to encompass the entire bulk of an amorphous sample,[12] the initial ordering of the random network has only recently been closely examined.[13,14]

In this paper we have used extended x-ray-absorption fine-structure (EXAFS) and Raman scattering to investigate structural changes before the onset of crystallization. Raman scattering was used to provide evidence of improved order and set an upper limit on the volume fraction of crystallinity after heat treatment.[15] For the Raman measurements growth kinetics were used to extrapolate the volume fraction of crystallinity as determined by the presence of the crystalline transverse-optical (TO) peak to values below the detectable limit. We present direct quantitative information on the ordering of a-Ge prior to the onset of crystallization as evidenced by a decrease in the bond-angle variation where the upper limit of the volume fraction of crystallinity, x, is less than 10^{-3}. Having established that the samples of interest were amorphous and single phased, it is then possible to interpret the EXAFS data in terms of structural parameters such as the bond-angle variation solely related to the amorphous network. We measured the temperature dependence of EXAFS taken on samples of a-Ge after various postdeposition furnace anneals. From the analysis of the transform of a-Ge EXAFS, we arrive at an upper bound for the mean-square deviation in the second-neighbor bond distance $(\Delta\sigma_2)^2$ and from that we calculate the spread in bond angle $\Delta\theta$ for each sample. The results corroborate the earlier Raman results and provide quantitative evidence of the ordering of these random networks prior to crystallization.

In Sec. II we present the sample-preparation particulars and a description of the Raman and EXAFS measurements. In Sec. III we present our results of the Raman and EXAFS analysis. In Sec. IV we discuss our results and quantify the disorder at various stages of anneal. We conclude in Sec. V.

II. SAMPLE PREPARATION, RAMAN SCATTERING, AND EXAFS MEASUREMENTS

Amorphous germanium samples 5—8 μm thick were sputtered onto 180-μm-thick quartz held at 20 °C. The heat treatment was performed in a tube furnace with flowing nitrogen at slightly above 1 atm pressure. Raman measurements were performed on the same samples subsequently used in the EXAFS studies. The heat-treatment time was set at 1 h for all samples.

Figure 1 shows the TO-phonon frequency (top) and the linewidth (bottom) versus the heat-treatment temperature obtained in the Raman experiments. Note that the peak frequency of the as-prepared sample is located at 267 cm^{-1} and increases to 274 cm^{-1} following heat treatment

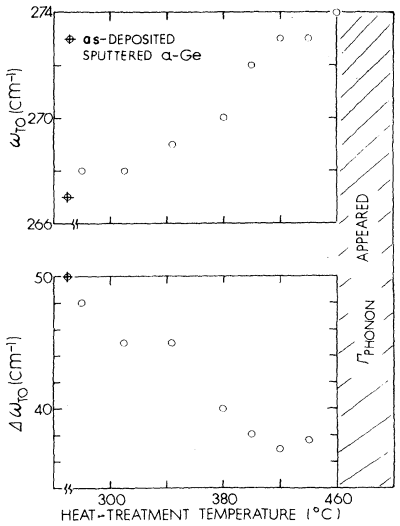

FIG. 1. Position (upper plot) and linewidth (lower plot) of the TO phonon in the Raman spectrum of a-Ge as a function of heat-treatment temperature. Appearance of the Γ phonon at 460 °C indicates a significant fraction of crystalline germanium ($\lesssim 3\%$).

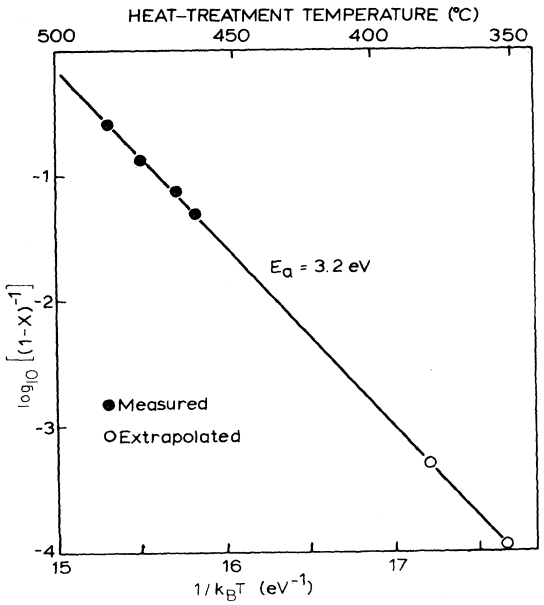

FIG. 2. Arrhenius plot of $\ln[1/(1-x)]$ where x equals volume fraction of crystallinity vs inverse temperature for a-Ge. Based on Raman measurements this technique can be used to determine crystallinity fractions well below the directly detectable limit. Technique is discussed in Ref. 15.

at 460 °C. On the other hand, the linewidth of the TO-phonon decreases from 50 cm^{-1} for the as-prepared sample to 37 cm^{-1} at 420 °C. The Γ-point TO phonon begins to appear at 460 °C, indicating the presence of crystallinity. It has been previously established that for this method the lower limit of the detectability of the volume fraction of crystallinity, x, is in the range of 3 vol %.[16] Thus it is not possible to find $x < 0.03$ for a given sample after heat treatment at a lower temperature, for example, 400 °C. In order to set an upper bound on x, we have further annealed the sample at 480 °C and followed the growth of the Γ-point TO-phonon peak. It is possible, by extrapolation, to obtain an estimate of x for samples annealed at 380 and 400 °C, i.e., the samples that were investigated by EXAFS. Figure 2 shows $\log_{10}1/(1-x)$ vs $1/k_BT$ where T is the heat-treatment temperature. The Arrhenius plot may be extrapolated to give the upper limit of $x \lesssim 10^{-3}$. Details of this procedure will be published elsewhere.[15] In this work we merely used the Raman scattering method to ensure that those anneal-stabilized a-Ge samples under investigation by EXAFS are almost totally amorphous and thus we are not reporting the results of EXAFS possibly arriving from a two-phase structure, microcrystallites embedded in an amorphous matrix.

Since our modeling has shown that the presence of microcrystallites would affect our interpretation only if there is more than 1 vol % volume crystallinity (an ordinate value of 10^{-2} in Fig. 2), the curve shown in Fig. 2 was used primarily to show that the fraction of microcrystallites present in our samples is *much* lower than this value even if very generous error bars are assigned to the data.

EXAFS measurements were performed at the Stanford Synchrotron Radiation Laboratory (SSRL) on the I-5 beam-line monochromator during a dedicated run, using a Si(220) channel-cut crystal. The beam energy was 3 GeV and beam currents were typically 40—60 mA. The samples were mounted in a variable-temperature cryostat. The temperature for the low-temperature data runs stayed at 80±1 K for all runs as monitored by a thermocouple and calibrated resistance thermometer.

III. EXAFS RESULTS

The individual data runs are identified using five character symbols, such as GeNT0. The Ge refers to the fact that the sample is germanium. The third and fourth characters refer to measurement temperature which may be either liquid-nitrogen temperature (NT) or room temperature (RT). The last character refers to annealing history which may be either unannealed (0), 380 °C annealed (3), or 400 °C annealed (4).

In Fig. 3 we present EXAFS taken at NT (approximately 80 K) for the three temperatures used in this study. The EXAFS for run GeNt3 [Fig. 3(b)] is considerably noisier than those of Figs. 3(a) and 3(c) and is distorted in the region around 6 Å^{-1}. This was caused by instabilities in the synchrotron during the run for GeNt3 and compromised the information which could be extracted from that case.

The Fourier transforms of the EXAFS data of Fig. 3 are presented in the next figure where runs GeNT0 and GeNT4 are shown in Figs. 4(a) and 4(b), respectively. All data were multiplied by k^3 before transforming them and the transforms were done over a $\vec{k}$-space range of 3.0—13.1 Å^{-1}. A measure of the noise level in these transforms can be obtained by viewing the size of features at large-r values., i.e., 6—10 Å, where a perfectly noise-

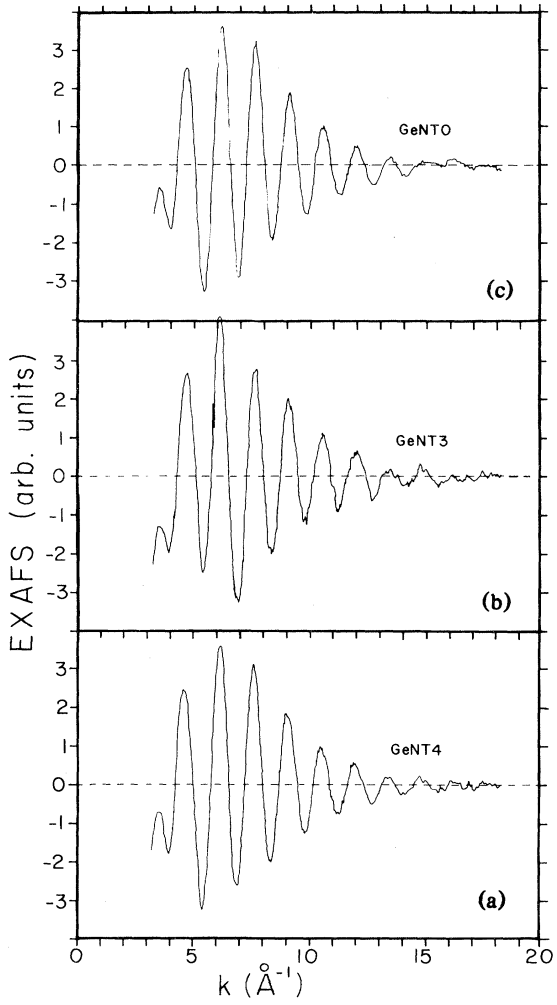

FIG. 3. EXAFS for a-Ge samples held at 80 K for various stages of heat treatment. From top to bottom, (a), (b), and (c) correspond to unannealed, 380 °C, and 400 °C 1-h anneals.

free transform would be zero. Similar transforms are shown in Fig. 5 for RT runs for which the noise levels are relatively low and similar for each run.

Finally in Table I we present results of the analysis of the first-neighbor peaks from the transforms for all six runs. We tabulate N_1, the coordination number for the first shell, and $\delta(\Delta\sigma_1)^2$, the relative change in mean-square deviations in the first interatomic distance. To obtain these data, first the EXAFS corresponding to the first-nearest-neighbor shell of the transforms was determined for all runs by filtering the transforms so that only contributions from the first shell remain. Then for each run the N_1 and $\delta(\Delta\sigma_1)^2$ values were calculated using two methods: the direct-ratio technique[17] and nonlinear curve fitting. For both methods, run GeNT0 was used as a standard presumed to have exactly four nearest neighbors. The parameters $\delta(\Delta\sigma_1)^2$ then correspond to the difference in $(\Delta\sigma_1)^2$ for the sample data relative to the standard. Similar results are obtained using each technique.

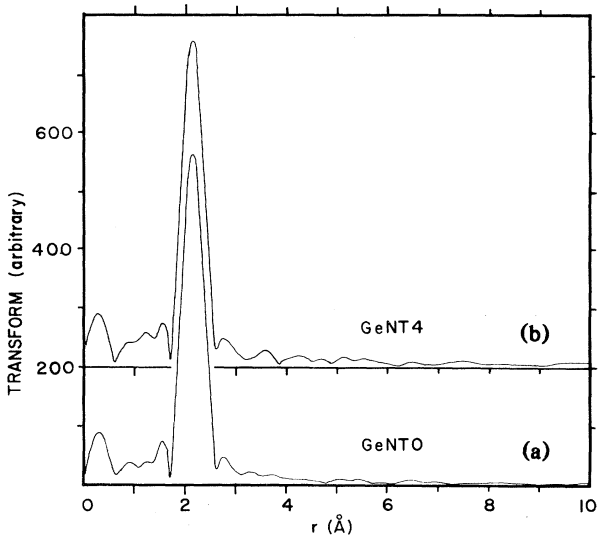

FIG. 4. Transforms of the EXAFS measured at 80 K for an unannealed (a) GeNT0 and a 400 °C-annealed (b) GeNT4 sample. Data were multiplied by k^3 and transformed over a range 3.5–13.1 Å. Feature at $r \simeq 3.6$ Å which rises above the noise only for GeNT4 results from the second-nearest-neighbor shell.

IV. DISCUSSION

Previous EXAFS results on amorphous germanium (a-Ge) have consistently shown no evidence of ordering past the first-nearest-neighbor peak.[18] Any indication of higher-shell ordering in transform data might be expected to occur at $r \simeq 3.7$ Å as seen in the transform for crystalline Ge (Fig. 6). We feel that evidence for such ordering does exist in Figs. 4(b) and 5(b). The noise level in

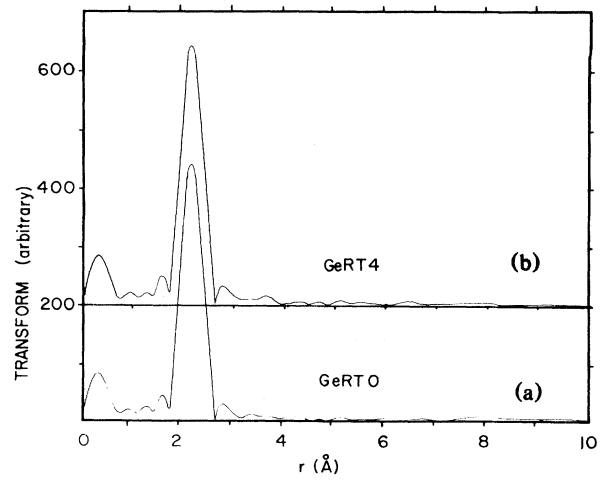

FIG. 5. Transforms of the EXAFS measured at RT for an unannealed (a) GeRT0 and a 400 °C (b) GeRT4 sample. The feature at $r \simeq 3.6$ Å which rises above the noise only for GeRT4 results from the second-nearest-neighbor shell.

TABLE I. Coordination number and relative mean-square spread in first-nearest-neighbor features of EXAFS transforms for all six spectra taken. GeNT0 is used as a standard in "ratio" and "fitting" calculations. Temperature dependence of the spread $(\Delta\sigma_1)^2$ is consistent with theory, as in the ordering of the first shell with annealing [a decrease in $(\Delta\sigma_1)^2$].

Run	Ratio N_1	Ratio $\delta(\Delta\sigma_1)^2$ (10^{-4} Å^2)	Fitting N_1	Fitting $\delta(\Delta\sigma_1)^2$ (10^{-4} Å^2)
GeNT0 standard	4.0	0	4.0	0
GeRT0	3.9±0.2	14 ±2	3.8±0.2	12 ±2
GeNT3	3.9±0.2	−2.3±4	4.0±0.4	0.4±4
GeRT3	4.0±0.2	15.1±2	3.9±0.2	13.7±2
GeNT4	3.8±0.2	−2.3±2	3.7±0.2	−3.9±2
GeRT4	4.2±0.2	12.7±2	3.9±0.2	12.3±2

these data is sufficiently low to distinguish these second-shell features, but the maxima at $r=2.8$ and 3.1 Å are satellites of the first-nearest-neighbor peak and should not be confused with higher-shell ordering. The feature near 3.6 Å, however, is not a satellite. Rather, it is evidence of higher-shell ordering. This conclusion is underscored by the persistence of the feature over several choices of transform ranges as illustrated in Fig. 7 where three transforms of the EXAFS of GeNT4 are shown. Here k_{max} refers to the maximum k values chosen. In all cases k_{min} was 3.50 Å^{-1}.

Figure 7 is best examined in light of Fig. 3(c), the EXAFS for GeNT4. For computational ease, zero crossings of the EXAFS were chosen as k_{max} values in determining the tranforms. The optimal zero-crossing choice for k_{max} is 13.05 Å^{-1} where the feature at $\sim$3.6 Å clearly rises above the noise. In Fig. 7, at $k_{max}=14.44$ Å^{-1}, the increased noise in the EXAFS adds sufficient high-frequency components to cause a diminution in the true second-shell feature. At $k_{max}=10.80$ Å^{-1}, the amount of noise incorporated into the transform is smaller, but signal information between 10.80 and 13.05 Å^{-1} is lost resulting in a decreased signal-to-noise ratio. Thus we use $k_{max}=13.05$ Å^{-1}.

For GeNT4 and GeRT4 all transform ranges resulted in a feature near 3.6 Å. The persistence of this feature lends credence to the conclusion that it represents a true nearest-neighbor shell. The evidence for this second-nearest shell in 380°C-annealed samples is not nearly as clear. The noise in Fig. 3(b) makes identification of a second shell in sample GeNt3 difficult, though the evidence is somewhat stronger for run GeRT3.

Just as Figs. 4 and 5 do show second-nearest-neighbor

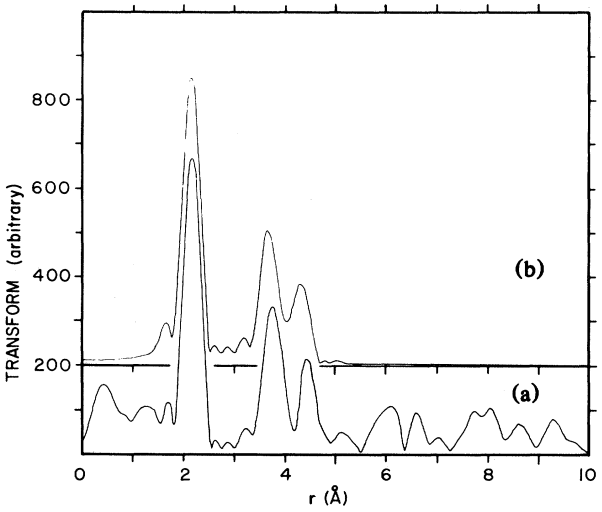

FIG. 6. EXAFS of crystalline germanium [(a), bottom] and a filtered transform [(b), top] for a model based on the same data with only first-, second-, and third-shell information. Filtered EXAFS on which (b) was based was used to model increasing amounts of disorder into a crystalline matrix. Resultant transforms are then compared to actual transforms from EXAFS obtained with annealed a-Ge.

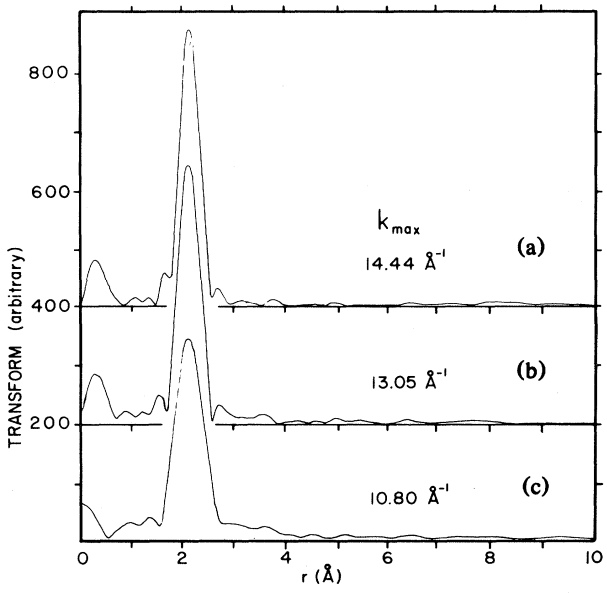

FIG. 7. Transforms of EXAFS of sample GeNT4 taken over different ranges. Maximum k value used in the Fourier transform is given in (a), (b), and (c) as 14.4, 13.05, and 10.80 Å^{-1}, reading from top to bottom. Increased noise incorporated into the transfer at $k_{max}=14.4$ Å^{-1} and a decrease in signal-to-noise ratio at $k_{max}=10.80$ Å^{-1} indicates that the intermediate value of 13.05 Å^{-1} is the indicated choice for k_{max}.

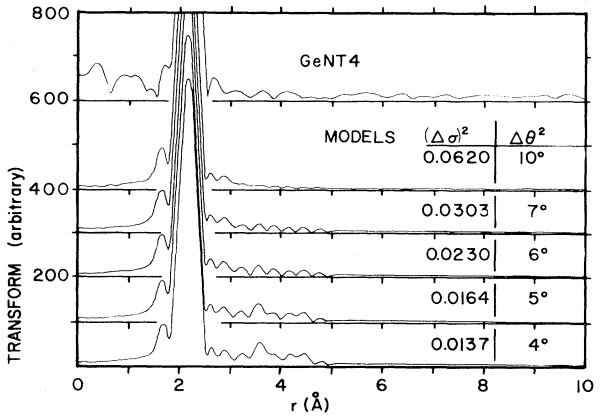

FIG. 8. Transform of the EXAFS of sample GeNT4 (top) and models of *c*-Ge incorporating decreasing amounts of disorder (bottom). Value of $(\Delta\sigma_2)^2$ corresponds to the spread (in Å^2) of the second-nearest neighbor introduced into the model filtered transform shown in Fig. 6(b). Angular spread for each of the five models is 10°, 7°, 6°, 5°, and 4°.

ordering for annealed samples, any evidence of higher shells is absent in the unannealed samples, GeNT0 and GeRT0 [Figs. 4(a) and 5(a)]. No strong features are seen in the transform of runs GeNT0 and GeRT0 for any range of frequencies chosen in the transformations.

The mean-square deviation of the second-nearest-neighbor distance $(\Delta\sigma_2)^2$ can give a measure of the bond-angle deviation $\Delta\theta$. To determine the $(\Delta\sigma_2)^2$ values which best fit our data we model the first three neighbor shells of a crystal and then introduce disorder by increasing the values $(\Delta\sigma_2)^2$ and $(\Delta\sigma_3)^2$. The crystalline results were modeled using the first shell of crystalline Ge as a model for all three shells. The result was that values of $(\Delta\sigma_2)^2=0.0014$ Å^2 and $(\Delta\sigma_3)^2=0.0018$ Å^2 relative to the disorder of the first shell gave the curve best fitting the crystalline results shown in Fig. 6(b). For successively larger disorder we show the resultant transforms [using Fig. 6(b) as a model] in Fig. 8. At the top of the figure, run GeNT4 is shown for comparison. Reading from the bottom up, the values of $(\Delta\sigma_2)^2$ used in the model calculations correspond to $\Delta\theta$ values of 4°, 5°, 6°, 7°, and 10°. Clearly our GeNT4 sample has a bond-angle distortion $\Delta\theta$, such that $4°<\Delta\theta<10°$. The features in GeNT4 in the range between 3 and 5 Å are best modeled by a total $(\Delta\sigma_2)^2$ value of 0.0303 Å^2. Thus the additional amount of disorder relative to the crystal is $0.0303-0.0014$ Å^2, or 0.0289 Å^2. The relationship between the mean-square deviation is second-nearest-neighbor distance and the spread in bond angle is given by

$$(\Delta\sigma_2)^2=(r_1\cos\tfrac{1}{2}\theta\, d\theta)^2 .$$

Using $r_1=2.45$ Å and $\theta=109°28'$ we calculate $\Delta\theta=7°$ for sample GeNT4.

Further confirmation of the determination of the value of $\Delta\sigma$ that best fits data can be made by comparing the peak height of the second-nearest-neighbor feature with model calculations. This is shown in Fig. 9 and Table II. We show at the top of the figure the entire crystalline transform from which the model was derived. At the bottom of the figure we show the second-nearest-neighbor feature incorporating increased bond-angle distortion. (For clarity only 1°—4° and 7° distortions are plotted.) In Table II we tabulate the peak height associated with this increasing disorder. With normalization of these values to the second-shell height in our data, we find a best fit for the 400 °C-annealed sample (GeNT4) to be $\Delta\theta=7°$.

The results of Table I show a temperature dependence of the spread of the first-nearest-neighbor shell consistent with theory.[19] In raising the temperature from 80 to 300 K, samples with each of the three annealing histories exhibit an increase in mean-square spreads $(\Delta\sigma_1)^2$ equal to 1.4×10^{-5} Å^2 within the error. The value quoted[19] by Chou *et al.* is 1.5×10^{-5} Å^2. Also Table I contains evidence that the first shell becomes slightly more ordered when annealed at 400 °C. For example, $(\Delta\sigma_1)^2$ decreases from 0 to $(-2.3\pm2)\times10^{-5}$ Å^2 from run GeNT0 to run GeNT4, where the minus sign indicates the sample is more ordered than the model compound. Once again, the data from the 380 °C-annealed sample are not as clear, but within the error, the 380 °C anneal exhibits first-shell ordering intermediate between unannealed and 400 °C-annealed samples for both ratio and fitting methods. This would imply that as the bond-angle variation decreases with annealing, there is a small decrease in the first bond-length distortion as well.

Although the crystalline state of Ge is structurally well defined, the amorphous "state" is actually a manifold of configurations of varying degrees of order representing many metastable states of free energy higher than the crystalline free-energy state. What we are observing in our experiments is the approach to very-low-free-energy configurations from which the final abrupt transition to the lowest-free-energy state—the crystal— can take place. Spaepen[7] modeled the amorphous-crystalline interface in *a*-Ge and determined the bond-angle distortion across this interface. His model incorporated a four-monolayer transition with a first and second amorphous layer and a first and second crystalline layer as one moved away from the interface in the amorphous and crystalline directions, respectively. Beyond the second crystalline layer, reasons Spaepen, material indistinguishable from bulk crystalline Ge exists. The transition from the amorphous bulk to the crystal involved these four layers.

EXAFS provides a particularly useful technique for measuring the final phase of ordering prior to crystallization in that slight increases in the bond-angle distortion $\Delta\sigma$ cause large effects in the EXAFS. Thus, in Fig. 9, increases in $\Delta\sigma$ from 0° to 7° results in a decrease in the second-nearest-neighbor peak to 4% of its original value. Comparison of this with Spaepen's second-amorphous-layer bond-angle distortion of 10° implies that both the theory and the experiment suggest that ordering of the amorphous network to its lowest-free-energy state involves a state incorporating 5°—10° of bond-angle distortion.

Ordering of the amorphous network involves not only decreasing the bond-angle distortion, but also aligning the dihedral angles since the perfect crystal exists in the stag-

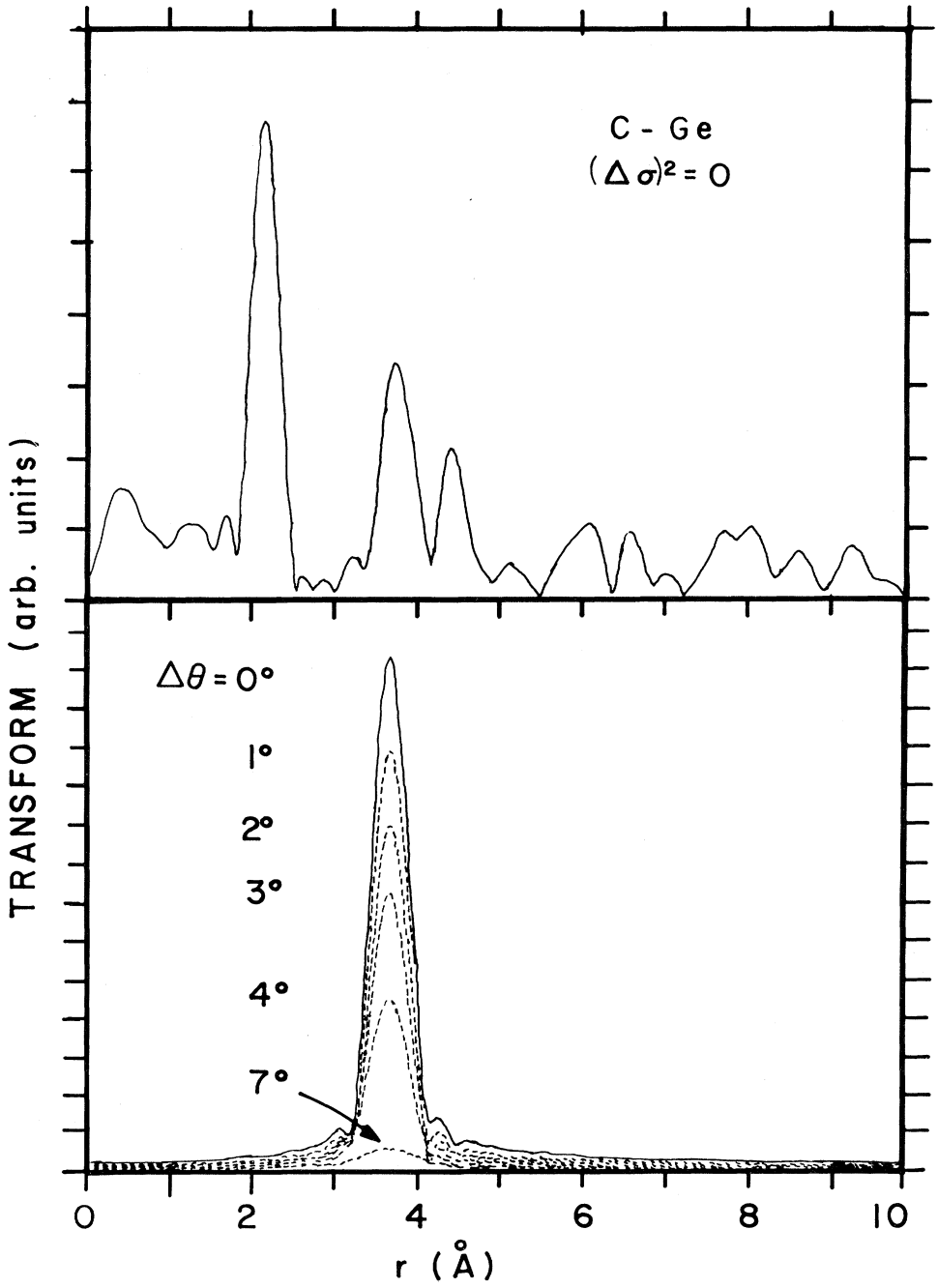

FIG. 9. Transform of the EXAFS of *c*-Ge (top) and a separately normalized filtered transform of the second-neighbor shell of the same EXAFS (bottom). Also included are model calculations based on the introduction of increased amount of disorder into the filtered transform. Disorder corresponds to angular deviations in the bond angle of 1°—4° and 7°. Height of each peak for each successive model is tabulated in Table II.

gered configuration. Pure dihedral ordering is, of course, not observable in EXAFS since it involves no change of first- and second-nearest-neighbor distances. Considering just two tetrahedra joined by one common bond in an eight-atom model it is easy to visualize that changes in the dihedral angle with no bond-angle distortion result in no change in the second-nearest-neighbor distance as a function of dihedral-angle changes. On the other hand, increased bond-angle distortion results in increased spread in the second-nearest-neighbor distance.

The angular approach to the lowest-energy amorphous state might be conceptually resolved into bond-angle or-

TABLE II. Peak height of second-nearest-neighbor feature in EXAFS transform as a function of increasing bond-angle disorder. Peak height is normalized to the crystalline transform [Fig. 6(a)].

$\Delta\theta$	$(\Delta\sigma)^2$ (Å^2)	Peak height
0° model	0	1.0
4°	0.0086	0.33
5°	0.0166	0.13
6°	0.0233	0.07
7°	0.0303	0.04
10°	0.0623	0.03
GeNT4	0.0312	0.05

dering and dihedral-angle ordering. For the three cases of purely dihedral-angle ordering, purely bond-angle ordering, and mixed bond-angle and dihedral-angle ordering, the former case can be ruled out by our EXAFS results. That is, if the ordering motion were principally an aligning of dihedral angles in a matrix with very little bond-angle distortion, the second-nearest-neighbor peak would be much stronger than it appears in Figs. 4 and 5. The weakness of any second-nearest-neighbor effects implies that the disordering involves substantial bond-angle disordering.

Modeling of the disorder of *a*-Ge has long been a topic of interest, and recent neutron-diffraction data has been used by Etherington and co-workers[20] to look critically at the various models.[21] The most successful correlations with experimental results are obtained for random-network models where strain energy has been minimized using a Keating potential. Even for these models, however, the second-neighbor peaks are much sharper than experiment, thus showing the distribution of bond angles to be too small. Etherington *et al.* conclude that this is a consequence of the model topology and arises because not enough strain energy was introduced into the models when they were built. For as-deposited *a*-Ge, Etherington *et al.* find $(\Delta\sigma_2)^2=0.078$ Å^2 and $\Delta\theta=9.7°$. Insofar as the absence of a second-nearest-neighbor peak on our as-deposited film sets and upper limit of $\Delta\theta\gtrsim 9°$ for our data, this null result is in agreement with Etherington. Our 400 °C-annealed sample may have a structure more consistent with the relatively relaxed structure of the models.

V. CONCLUSION

EXAFS measurements on annealed *a*-Ge indicate a decrease in the deviation of the first- and second-nearest-neighbor distances from the crystalline values with increased annealing temperature. We obtain first- and second-nearest-neighbor distances and a bond angle consistent with diffraction results, and from the decreases in the deviations of these distances we measure a bond-angle distortion of 7° and a slight tightening of the spread in the first-nearest-neighbor distance for the 400 °C-annealed sample. The approach to order—and indeed the transition to crystallinity—must involve decreases in bond-angle distortion. These EXAFS results, however, cannot in and of themselves rule out an increase in order due to an increasing fraction of microcrystals in an amorphous matrix.

Raman measurements performed on the same samples which are used in EXAFS experiments are noticeably more sensitive to changes with annealing. The measurements show a shift of the TO-phonon frequency and linewidth with increased annealing temperature. More importantly, the Raman results may be used to set an upper limit on the volume fraction of crystallinity in the 400 °C-annealed sample. This limit is 10^{-3}, so that the EXAFS measurements on this sample represent evidence of improvement in bond-angle deviation in the ordering of anneal-stabilized yet still amorphous germanium.

Thus our EXAFS-Raman experiment has shown that a relaxed amorphous phase of germanium—with a crystallinity fraction of less than one part in a thousand—can be obtained by annealing thin evaporated films. The mean-square deviation of the bond angle for such samples is 7°. Since modeling of *a*-Ge has consistently shown more order than experimental diffraction results, a confirmation of our results accomplished by diffraction studies on similarly prepared films might result in a diffraction-modeling correlation in better agreement than that currently in the literature.

ACKNOWLEDGMENTS

We gratefully acknowledge John Rehr for useful discussions and data prior to publication. Work done at SSRL which is supported by the National Science Foundation through the Division of Materials Research and the National Institutes of Health through the Biotechnology Resource Program in the Division of Research Resources (in cooperation with the U.S. Department of Energy). This work was supported in part by Standard Oil (Ohio) Corporation. One of us (M.A.P.) acknowledges the support of the General Electric Corporation.

[1]Marc Kastner and H. Fritzsche, Mater. Res. Bull. 5, 631 (1970).

[2]S. C. Agarval, Phys. Rev. B 7, 685 (1973).

[3]S. J. Hudgens, Phys. Rev. B 7, 2481 (1973).

[4]M. A. Paesler, in *Proceedings of the Vth International Conference on Amorphous and Liquid Semiconductors,* edited by J. Stuke and W. Brenig (Taylor and Francis, London, 1974), p. 229.

[5]*Laser and Electron-Beam Solid Interaction and Materials Processing,* edited by J. F. Gibbons, L. D. Hess, and T. W. Sigmon (North-Holland, New York, 1981).

[6]T. Takamori, R. Messier, and R. Roy, Appl. Phys. Lett. 20, 201 (1972).

[7]F. Spaepen, Acta. Metall. 26, 1167 (1978). F. Spaepen and D. Turnball, in *Laser-Solid Interactions and Laser Processing—1978* (Materials Research Society, Boston), Proceedings of the

Symposium on Laser-Solid Interactions and Laser Processing, edited by S. D. Ferris, H. J. Leamy, and J. M. Poate (AIP, New York, 1979), p. 73.

[8]*Proceedings of the Materials Research Society Annual Meeting, Boston, Massachusetts, 1982* (Elsevier, New York, 1983), Vol. 13, p. 135.

[9]J. C. Phillips, J. Non-Cryst. Solids 35-36, 1157 (1980).

[10]K. Tanaka and R. Tsu, Phys. Rev. B 24, 2038 (1981).

[11]M. F. Thorpe (unpublished).

[12]See, for example, P. Germain, S. Squelard, J. Bourgoin, and A. Gheorgheu, J. Appl. Phys. 48, 5 (1977); F. Evangelisti, M. G. G. Prioetti, A. Balzarotti, F. Comin, L. Incoccia, and S. Bolilio, Solid State Commun. 37, 413 (1981).

[13]S. T. Kshirsagar and J. S. Lannin, J. Phys. (Paris) Suppl. 12, C6-54 (1981).

[14]R. Tsu, J. G. Henandez, J. Doehler, and S. R. Ovshinsky, Bull. Am. Phys. Soc. 27 (3), 207 (1982).

[15]J. G. Hernandez and R. Tsu, Appl. Phys. Lett. 42, 90 (1983).

[16]R. Tsu, J. G. Hernandez, S. S. Chao, S. C. Lee, and K. Tanaka, Appl. Phys. Lett. 40, 534 (1982).

[17]J. W. Cook, Jr. and D. E. Sayers, J. Appl. Phys. 52, 5024 (1981).

[18]T. Hayes, in *Atomic Scale Structure of Amorphous Solids,* edited by G. S. Cargill and P. Chaudhair (North-Holland, New York, 1979).

[19]S. Chou, B. A. Bunker, and J. J. Rehr (unpublished).

[20]G. Etherington, A. C. Wright, J. T. Wenzel, J. C. Dore, J. H. Clarke, and R. N. Sinclair, J. Non-Cryst. Solids 48, 265 (1982).

[21]See, for example, D. E. Polk and D. S. Boudreaux, Phys. Rev. Lett. 31, 92 (1973); G. A. N. Connell and R. J. Temkin, Phys. Rev. B 9, 5323 (1974); D. Beeman and B. L. Bobbs, Phys. Rev. B 12, 1399 (1975); Refs. 2—20 in Ref. 20.